BC from fungus chaff: an unexpected adsorbent for methylene blue removal

Yingjie Dai, Xu Zhang, Xiaorou Wang, Qinyi Xiong, Qi Liu, Wei Zhao*

College of Resources and Environment, Northeast Agricultural University, No. 600 Changjiang Road, Xiangfang District, Harbin 150030, China, Tel. +86 451 5519 0825; Fax: +86 451 5519 0825; emails: dai5188@hotmail.com (W. Zhao), dai5188@gmail.com (Y. Dai), 272164193@qq.com (X. Zhang), xiaorouwang77@163.com (X. Wang), qinyixiong@126.com (Q. Xiong), 918212673@qq.com (Q. Liu)

ABSTRACT

Methylene blue (MB) was a standard indicator used to evaluate adsorption. The biochar (BC) was prepared from the combustion of waste chaff in fungus farm. The influence of contact time, initial pH, adsorbent dose, the adsorption isotherms, contact temperature, ionic strength, and regeneration of BC was determined. The removal ratios of MB for three kinds of chaff BC shown in the results of this report after 6 h were 94.27% (BC700), 85.47% (BC500), and 70.28% (BC300), respectively. According to the saturated adsorption capacity of the Langmuir isotherm, the parameter value of MB was obtained (Q_0): 7.75 mg/g for BC700; 6.37 mg/g for BC500, and 5.18 mg/g for BC300, respectively. The optimal level of adsorption, in this report, for MB ions was provided by BC700. It could be attributed to hydrophobicity, hydrogen bonding, and π–π interaction.

Keywords: Adsorbent; BC; Fungus chaff; Kinetics; Pyrolysis

1. Introduction

Methylene blue (MB) is generally used in the industrial production and textile industries. MB compounds are inexpensive and easy to prepare, so it is used in the dyeing process [1]. Moreover, MB is also used as a drug, such as antidepressants and antimalarials. MB can treat encephalopathy, which is due to toxin-induced isoprene. In addition, MB can inhibit heavy metal corrosion and detoxify cyanide [2]. MB is chemically stable and requires many years of degradation under natural conditions. Methylene blue is discarded during paper and textile processes [3]. A large amount of MB enters the ecosystem and causes serious adverse effects on the natural environment [4–6]. In addition, at higher concentrations, MB can be biodegraded. At the same time, MB is toxic to aquatic organisms. It can block sunlight from entering the water body and has high thermal stability [7]. The random discharge of MB has brought greater environmental harm [8]. In various methods of treating sewage, adsorption is currently widely used because of its simple design, easy operation, and good treatment effect [9]. Among the adsorption methods, activated carbon, as its excellent adsorption effect, becomes one of the most widely used adsorbents. However, in production and life, activated carbon has defects such as high production cost and difficulty in regeneration. These defects limit its scope of use [10]. So many researchers have recently explored some low-cost adsorbents [11]. Biochar (BC) have been extensively studied by pyrolysis at appropriate temperatures and in an oxygen-limited environment [12]. The removal rate of Congo red in water by BC prepared from algae residues was as high as 82.6% [13]. Some scholars studied the adsorption behavior of corn cob-based BC on MB and found that 600°C BC had higher aromaticity and hydrophilicity, and the main adsorption mechanisms are π–π interaction and hydrogen bond [14]. Some studies have shown that Ginkgo biloba BC (GBBC) has a better adsorption effect on MB. The results show that GBBC can

* Corresponding author.

be used as an excellent material for adsorbing MB characterized by a wide adaption range of pH (2.0–12.0) and short sorption equilibrium time (30 min) [15]. Some studies have shown that the specific surface area of BC is 2,892.70 m²/g, the total pore volume is 1.28 cm³/g and the micropore volume is 0.42 cm³/g, which is indicated that the prepared BC materials are mainly microporous [16]. At the same time, some studies have found that several modified BCs have good adsorption capacity, but they require higher pyrolysis temperatures [17,18]. The above studies show that BC has a high specific surface area and strong hydrophobicity. The characteristics allow MB adsorbed on BC to have the advantages of short adsorbing time and large adsorbing capacity. The main adsorption mechanism of BC is hydrophobicity and π–π interaction.

The chaff is an agricultural waste produced by the production of fungus. At present, the annual production of fungus chaff in China is more than 10 million tons [19]. The chaff loses its value of agricultural production and is discarded in large quantities. This not only caused the waste but also polluted the environment. The components of the fungus chaff are mainly materials including sawdust, wheat bran, soybean powder, gypsum, brown sugar, and water. The components were mixed in the corresponding proportions as shown in Figs. 1 and 2. And they were stirred for 30 min. The material is bagged. The fungus chaff is sterilized at 105°C for 6–8 h under normal pressure. Then, the black fungus is inoculated into the bag at an ambient temperature of 18°C–25°C and humidity of 50%–70%. Black fungus is harvested two times in May and September each year. The fungus bag is discarded as an agricultural waste after 1 y of use. Some studies found that under the condition of alkaline (pH = 7.0), when the dosage of modified fungus chaff is 2.0 g/L and the initial concentration of MB is 100 mg/L, the decolorization rate of modified fungus chaff to MB can reach 60.37%, and the saturated adsorption

capacity can reach 14.81 mg/g [20]. The decolorization rate of MB in water by the unmodified fungus chaff as an adsorbent was only 75.14% [20]. Some studies found that adsorption of crystal violet on fungus chaff has majored in a single layer [21]. The above studies show that the fungus chaff had a certain adsorption capacity. But the adsorption capacity is low. At the same time, fungus chaff can pollute water body and cause secondary pollution in the process of wastewater treatment. Some studies have shown that there is no secondary pollution of BC produced from fungus chaff in wastewater treatment. The research direction of chaff BC is mainly to improve soil quality. Removal of MB from the water with fungus chaff BC as an adsorbent was reported rarely. In existing reports, the adsorption capacity of MB in water on fungus chaff BC prepared by hydrothermal method can reach 164.44 mg/g [22]. This shows that the fungus chaff BC, as an adsorbent, has a great advantage in removing MB in water. Although some recent studies have shown the feasibility of using activated carbon as raw material to prepare BC [23]. However, the above report also only explored the preparation process. In this work, there is a lack of research on the actual adsorption of MB in water by fungus chaff BC. At the same time, there is almost no research on the MB removal in water onto fungus chaff BC prepared by pyrolysis method similar to this study. In summary, this study has great research value. Fungus chaff BC as an adsorbent has great innovation in removing MB in water.

In this study, BCs prepared by using fungus chaff as raw materials adsorbed MB in water. It made the chaff waste recycle and provided an innovative way to the disposal of MB wastewater. It reported the influence of three BCs' adsorption behavior and surface group on MB. Some parameters' influence such as structural characteristics of samples, adsorbent dose, contact time, ionic strength, initial pH, and regeneration were investigated. From batch
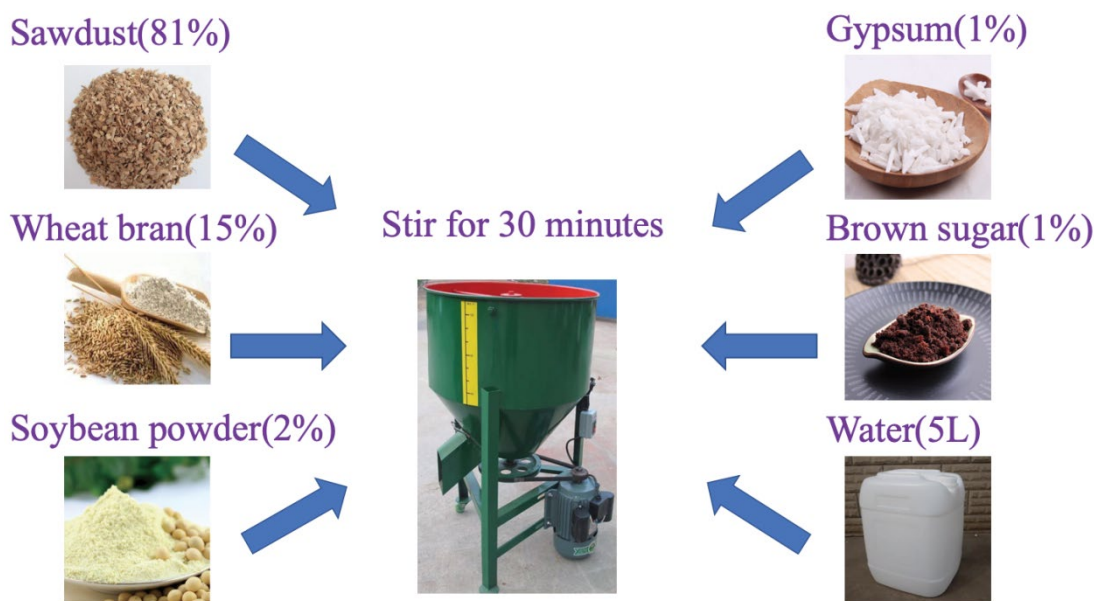

Fig. 1. Preparation of fungus chaff.

Fig. 2. Sterilization of fungus chaff, culture of black fungus, and production of waste fungus chaff.

experiments, the adsorption equilibrium and kinetics of MB for BCs were obtained. On the surface functional groups of BCs, the adsorption mechanism of MB was analyzed. The research results can enrich waste resources and provide a new way to remove MB-containing wastewater.

2. Materials and methods

2.1. Materials

In a laboratory at the Northeast Agricultural University, the samples, in this study, were prepared during thermal pyrolysis of fungus chaff. During the summer of 2018, the fungus chaff used in this experiment were obtained from the fungus farm in the Greater Khingan Range, Heilongjiang (after approximately 1 y of use) of China. Firstly, the fungus chaff was dried and crushed. Subsequently, the dried fungus chaff was pyrolyzed at three temperatures (300°C, 500°C, and 700°C) to prepare BC. For three temperatures, the time of pyrolysis was 2 h. In a muffle furnace, the BCs were collected from the crucible. BCs were dried and crushed before using. The prepared chaff carbon was labeled BC. In this study, all chemicals were pure. These chemicals were made from distilled water.

2.2. Chemical characteristics and physical of BC

The surfaces of BCs were observed under S-3400 N (Hitachi Ltd., Tokyo, Japan) and a low-vacuum scanning electron microscopy (SEM). The XRD patterns were characterized by Bruker D8 Advance (Bruker Co., Berlin, Germany). We used the method which had been determined by Boehm to measure the number of basic areas and acidic function groups on the surface of the BC. Acidity was determined in a well-sealed flask by mixing 0.5 g of either BC with 15 mL of NaOH (0.1 mol/L), Na_2CO_3 (0.05 mol/L), or $NaHCO_3$ (0.1 mol/L) solution. The mixture was shaken at

25°C and 165 rpm for 48 h. The samples were titrated using HCl (0.1 mol/L). The carboxylic group on the surface of BCs reacts only with $NaHCO_3$. The carboxylic and lactone groups are reacted with Na_2CO_3. The carboxylic group, lactone group, and phenolic group reaction can react with NaOH. Therefore, the amount of $NaHCO_3$ minus the amount of Na_2CO_3 is equal to the amount of lactone groups, and the amount of Na_2CO_3 minus the amount of NaOH is the number of phenolic groups. The alkalinity was measured like that described above. However, the sample was titrated with HCl (0.1 mol/L), and then residual HCl was titrated with NaOH (0.1 mol/L). The method of Leon et al. [24] was used to determine the zero charge point (pH_{PZC}) of the samples.

2.3. Adsorption kinetics

The pseudo-first-order kinetic model and the pseudo-secondary model are used to describe the kinetic process of the adsorption process on the BC surface. The following is the rate equation:

$$\frac{dq_t}{dt} = \left(q_e - q_t\right)^n \tag{1}$$

In Eq. (1), q_e represents the saturated adsorption amount, that is, the amount of MB (mg/g) adsorbed per unit mass of the adsorbent when the adsorption reaches equilibrium. Q_t represents the amount of MB (mg/g) adsorbed at time t. k_n is an nth order rate constant. When $n = 1$, the unit of k_n is 1/min. When $n = 2$, the unit of k_n is g/mg min. Linearize the equation to obtain the following equation:

$$\ln\left(q_e - q_t\right) = \ln q_e - k_1 t \tag{2}$$

$$\frac{t}{q_t} = \frac{1}{k_2 q_e^2} + \frac{t}{q_e} \tag{3}$$

According to the relationship diagram of $\ln(q_e - q_t)$ vs. t, and the correlation coefficient (R^2) and rate constant (k_n) of the first-order dynamic model can be determined. The line graphs of t according to t/q_t are used to determine the correlation coefficient (R^2) and rate constant (k_n) of the second-order kinetic model, respectively. The fitting equation and the values of R^2 and q_e were determined by linear regression.

2.4. Adsorption experiment

This study investigated some parameters that affect BC adsorption, such as initial pH, contact time, adsorbent dose, ionic strength, and regeneration. From experiments, kinetics and adsorption equilibrium were obtained by using adsorbents and 25 mL of 10 mg/L MB solution. The adsorption isotherms were discussed. It was implemented by using 25 mL of MB solution (6–20 mg/L) and adsorbents. The adsorbents were separated from MB solution via centrifuge at 4,600 rpm for 15 min (use IEC61010–2–020, KUBOTA, Japan) after equilibrium. Using a UV spectrophotometer V550 (Jasco Co., Tokyo, Japan), the operating wavelength was adjusted to 665 nm, and the standard operating curve of MB was obtained. Searching for the standard working curve, we could get the corresponding MB concentration under different absorbance. The specified pH environment required for the experiment was achieved with 0.1 mol/L HCl or 0.1 mol/L NaOH. The adsorbent dose was 0.8–3.0 g/L. The added MB concentration was from 6 to 20 mg/L. The contact time was from 1 to 12 h. The temperature during the adsorption process was always maintained at 25°C. Three times for each experiment, the average of the results obtained from the three experiments was calculated. The standard deviation of the MB determined in this way is about 5%. The specific surface area of BC was evaluated using N_2 at –196°C (Micromeritics Gemini VII 2390p, Norcross, USA). The Nalyser TG-151 analyzer was used to analyze the preparation process of BC. The reaction chamber was separated from the furnace chamber by an internal quartz tube (inner diameter of 34.5 mm). The fungus chaff was placed in a quartz sample pan for experiments. The heating rate was consistent with the heating rate in the BC preparation process described above. Fourier transform infrared (FTIR) spectra (Nicolet FTIR 6700, USA) of BCs in the spectral range of 4,000–400 cm⁻¹ were used to evaluate the surface functional groups of BCs. Under the action of the agate mill, the powdered BC is evenly mixed with anhydrous KBr (1:800). By grinding, the diameter of the mixture can reach 13 mm. The prepared mixture is placed in a sample chamber of an infrared spectrometer. According to the above experimental steps, the infrared spectrum of BC was obtained.

3. Results and discussion

3.1. Chemical characteristics and physical of the samples

The SEM images of BC300, BC500, and BC700 are shown in Fig. 3. The surface structure of BCs and the porosity were shown. The BCs have higher adsorption efficiency due to its larger porosity and specific surface area.

The BCs SEM images revealed layered structure or structures a partial blocky. From BC300 to BC700, the surface structure of BC appeared many collapses that of
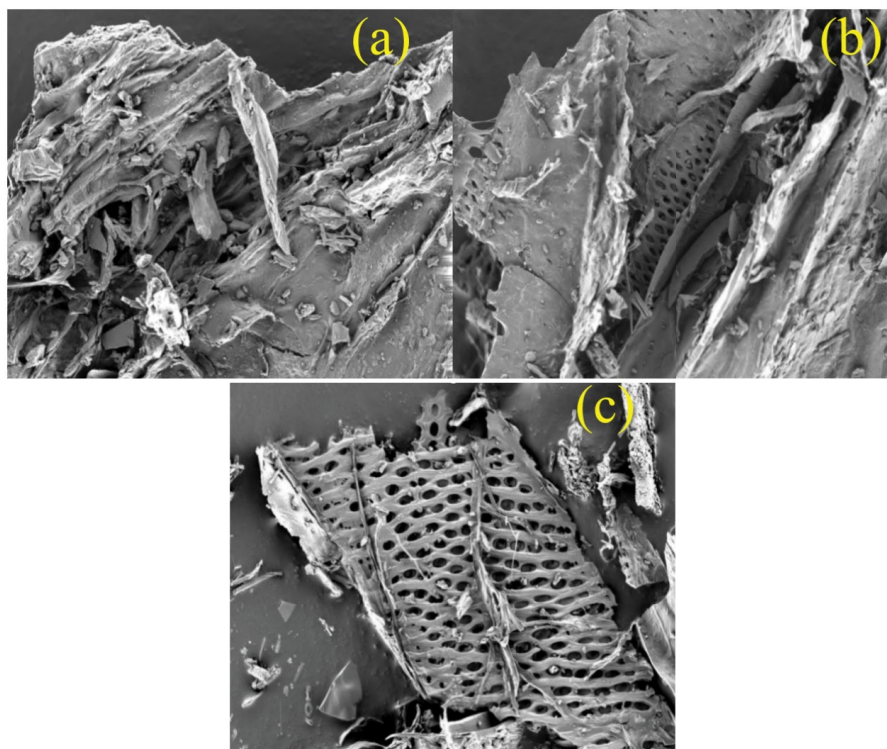
Fig. 3. SEM images of the BC300 (a), BC500 (b), and BC700 (c).

honeycomb structures. With the highest porosity, BC700 showed a large number of micropores and mesoporous pores. At the same time, the surface of the BCs at the three pyrolysis temperatures is rough, which created a good environment for adsorption. To study the polarities of BCs, we measured pH_{PZC} and basic and acidic functional groups (Table 1a). BC micropore space can be filled with many oxygen-containing functional groups [25]. As the pyrolysis temperature gradually increases, the number of acidic functional groups decreased (from 1.08 to 0.71 mmol/g), which also reasonably explained the phenomenon of porosity increasing with the increase of pyrolysis temperature in the SEM diagram. At the same time, with the acidic functional group decreased, the hydrophobicity of BC significantly increased. On BC, it is good for MB removal. Finally, with the increase of pyrolysis temperature, the number of functional groups that adsorb is greatly increased. The number of surface basic functional groups of BCs gradually increased as the pyrolysis temperature increases. In the graphite layer structure of carbon, the electron-rich region is one of the important factors for increasing the surface functional groups [26]. As the enrichment of a great deal of basic functional groups, the pH_{PZC} values of three BCs were greatly increased from 6.43 to 7.70. Depending on the relationship between the true pH, these results show that the surface charge of BC was negative or positive.

Figs. 4-1 show the FTIR spectra of BC300, BC500, and BC700. Analysis of the images shows that as the pyrolysis temperature increases and after adsorption, the peaks of some surface functional groups gradually decrease. Firstly, as the pyrolysis temperature increases, the peaks of the phenolic group (–C–OH) at 1,405 cm^{-1} and the phenolic group (–C–OH) at 1,116 cm^{-1} of the initial BC surface decreased, respectively. The position of benzene moved from 3,407 cm^{-1} of BC300 to 3,432 cm^{-1} of BC700. This shows that as the pyrolysis temperature increases, the carbonization degree of BC gradually increases. Secondly, the FTIR of three BCs before and after the BC adsorbed MB had different trends. The comparison of the images before and after BC300 adsorption showed that the peak of the phenolic group (–C–OH) at 1,405 cm^{-1} decreased significantly. Similarly, the images can show that the carboxylic and benzene peaks at 1,700 and 3,432 cm^{-1}, before and after adsorption, have

Table 1a
Physical and chemical properties of adsorbents

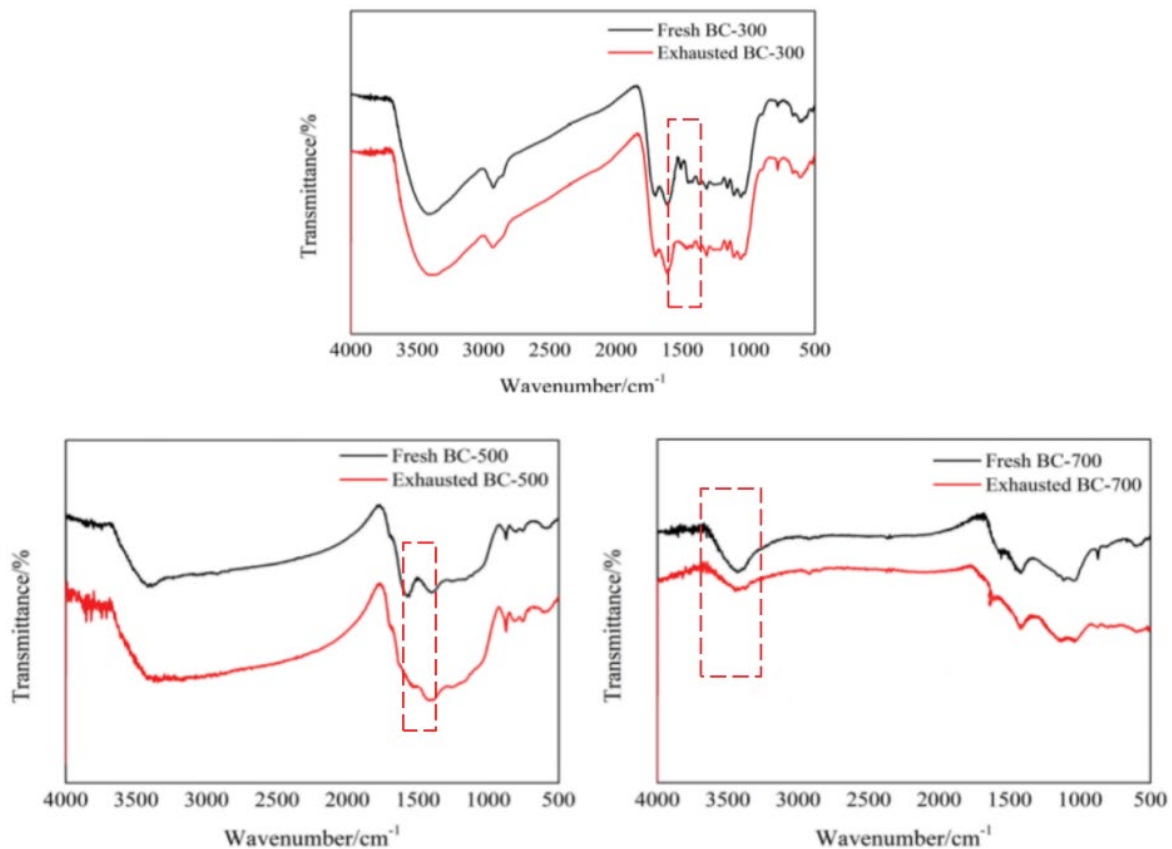| Samples	BC700	BC500	BC300
Acidic functional groups (mmol/g)	0.71	0.84	1.08
Carboxylic groups (–COOH)	0.33	0.35	0.35
Lactone groups (–COO–)	0.15	0.23	0.28
Phenolic groups (–OH)	0.23	0.26	0.36
Basic functional groups (mmol/g)	0.83	0.91	0.54
pH_{PZC}	7.70	7.53	6.43

Fig. 4-1. FTIR spectra obtained for BC300, BC500, and BC700.

significant downward trends, respectively. This indicates that the adsorption mechanism of BC300 may involve the formation of hydrogen bonds between the phenolic groups on the surface of BC and MB. At the same time, the high aromaticity of BC500 and the decrease of the peak value of acidic functional groups may increase the surface polarity of BC. Therefore, the π–π interaction between BC500 and MB is enhanced. This may explain the adsorption mechanism of MB on BC500. The trend of BC700 benzene peak movement and decline also indicates that the adsorption mechanism of BC700 may involve a hydrophobic effect.

Tables 1b show the measurement results of the Brunauer–Emmer–Teller (BET) correlation coefficient of BCs. The specific surface area and pore volume of BC700 are 46.56 m²/g and 0.06 cm³/g, respectively. Compared with BC500 and BC300, they are both at a higher level. As the pyrolysis temperature increases, the BET surface area of BC also increases. Previous studies have also been reported

Table 1b
Textural analysis of BCs

Samples	BET surface area (m²/g)	Pore volume (cm³/g)	Average of pore width (nm)
BC300	2.55	0.012	80.70
BC500	18.95	0.035	16.21
BC700	46.56	0.060	3.00
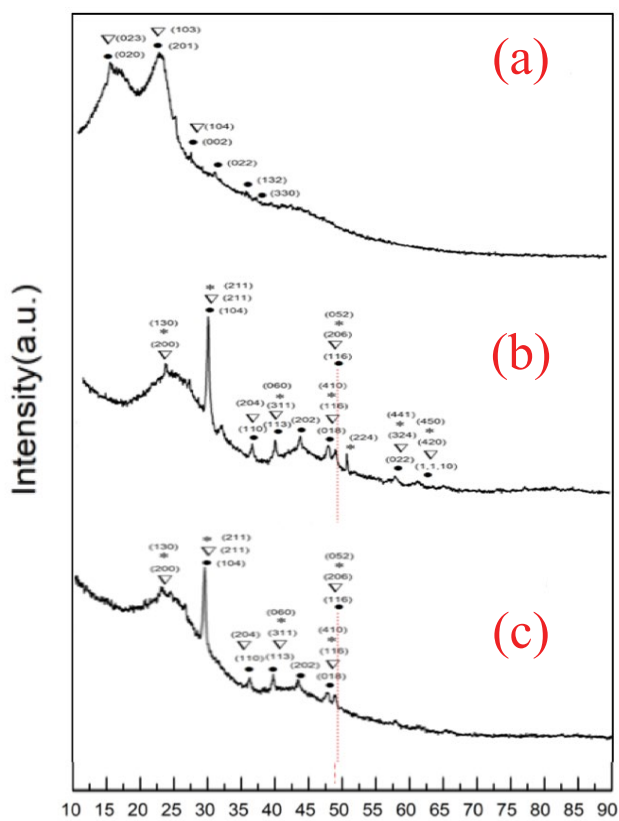
[27]. Higher BET surface area and larger pore volume are more favorable for BC and MB adsorption.

The crystal structure of the adsorbent BC can be analyzed by XRD. As shown in Fig. 4-2, BC exhibited strong and sharp peaks at 2θ = 23.9° and 26.9° and 2θ = 16.5°. This showed that BC is similar in nature to quartz and calcite, similar to previous studies on BC, such as reed derivatives [28]. According to the results of the absorption peaks in X-ray diffraction (XRD), the calcite in the BC sample was partially decomposed as the pyrolysis temperature increased [29]. These results may be due to the presence of dust on the material that is left by atmospheric deposition [30]. According to the results of XRD, dolomite and quartz (CaMg(CO$_3$)$_2$, 2θ = 35.2° and 46.3°) were present inside. Similar findings were found in other studies [31]. At the same time, XRD analysis showed that it had a non-uniform surface [32]. However, the XRD patterns of the samples were quite different. As shown in Fig. 5 as the pyrolysis temperature gradually increases, the peak between 15° and 25° in the XRD pattern becomes wider. It indicates that the carbon content in the BC sample is high and the crystallinity of this phase was poor [33]. The three images had distinct diffraction peaks at 2θ = 24°, respectively. This showed that all three BCs have locally ordered carbon layers. At 2θ = 43°, the aromaticity increased with the increase of peak value. According to the image, the aromaticity of the samples increased with increasing temperature. This also explains that there may be some π–π interaction between the two BCs (BC700 and BC500) and MB. However, the weak aromaticity of BC at 300°C also indicated that π–π interaction was not the main adsorption mechanism.

As shown in Fig. 4-3, the air-dried fungus chaff has less water, so the heat loss curve is smoother at 100°C–200°C. The mass-loss rate of BC is basically less than 3%. In the temperature range of 200°C–400°C, a second platform of BC weightlessness appeared. BC's mass loss rate is about 18%. Among the three main chemical components of fungus chaff, hemicellulose is the most easily pyrolyzed, cellulose is the second and lignin is the most difficult to pyrolyze. It can be speculated that the thermogravimetric analysis (TGA) platform appearing in this temperature range is mainly due to a large amount of decomposition of cellulose and hemicellulose. 330°C–360°C is the aliphatic side chain

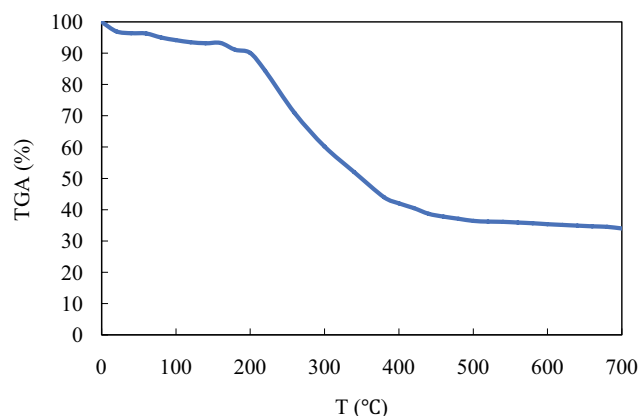Fig. 4-2. XRD images of the BC300 (a), BC500 (b), and BC700 (c).

Fig. 4-3. TGA curve for BC.

and hydrogen-bonded hydroxyl cleavage. Partial aromatic cleavage occurs at 438°C and higher. According to Fig. 4-3, it can be seen that the mass loss rate of BC is gradually increasing in the two temperature change intervals. This shows that the functional groups on the BC surface are gradually decreasing. This agrees with the results of FTIR and surface functional groups. When the temperature is between 500°C and 700°C, the change in mass-loss rate is low. So BC700 has higher stability and BC300 has poor stability.

3.2. Adsorption kinetics

As can be seen from Fig. 5, the effect of contact time on BC adsorption of MB. The removal ratios of MB after 6 h were 94.27% for BC700, 85.47% for BC500, and 70.28% for BC300, respectively. As contact time increases, the absorption rate of MB by the three adsorbents gradually increased and reached a peak after 6 h. According to the experimental data, the adsorption process and adsorption kinetics could be evaluated. To better describe the mechanism of adsorption, we used first-order and second-order fitting models to predict the data. The effect diagram of the pseudo-second-order dynamics model fitting is shown in Fig. 5. According to the kinetic constants in Eqs. (1) and (2), the parameters in the formula could be derived. These parameters are shown
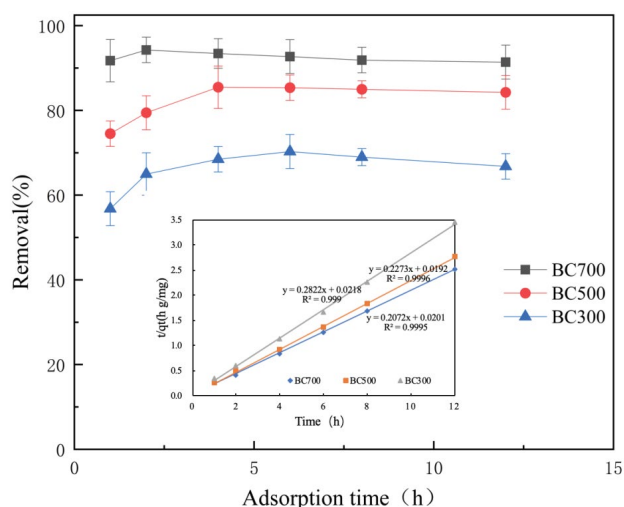

Fig. 5. Effect of adsorption time by three BCs: MB removal (C_0 = 10 mg/L, adsorbent dose = 2.0 g/L, at pH = 7.0 and 25°C).

in Table 2. The data does not conform to the variation law of the pseudo-first-order model. The experimental results differ greatly from the q_e values fitted according to the pseudo-first-order model. Therefore, the pseudo-first-order kinetic process cannot correctly describe the adsorption process of MB to BC. Moreover, the R^2 of the pseudo-second-order dynamic model is higher, which better indicated that the adsorption process is consistent with the pseudo-second-order model. The R^2 of the three materials are 0.9990 for BC300, 0.9996 for BC500, and 0.9995 for BC700, respectively. The calculated q_e values of BC700 (4.83 mg/g), BC500 (4.40 mg/g), and BC300 (3.54 mg/g) were in compliance with the experimental data (4.85 mg/g for BC700, 4.40 mg/g for BC500, and 3.62 mg/g for BC700), respectively. Therefore, it showed that the adsorption was more prone to pseudo-secondary adsorption. According to the fitting of the two kinetic models, the adsorption mechanism of this experiment not only has physical adsorption but also chemical adsorption. The chemical adsorption of MB on BCs was stronger than physical adsorption. This was consistent with the results obtained by XRD. Both results indicated that hydrogen bond, π–π interaction, and hydrophobicity might be the main adsorption mechanism of BCs.

3.3. Effect of solution pH

A series of MB absorbance values were determined using an ultraviolet spectrophotometer. The spectrophotometer was tested using a stoppered bottle containing 25 mL of 10 mg/L MB solution, which were regulated by strong acid solution and strong alkaline solution to pH value of 3.0, 5.0, 7.0, 9.0, and 11.0 at 50 mg of adsorbents at 165 rpm and 25°C. The pH was regulated to the required value by using 0.1 mol/L NaOH or 0.1 mol/L HCl per hour in the whole test. In the adsorption of MB, studies had indicated that pH was not a significant factor. The effect of pH on MB adsorption BC was indicated in Fig. 6. With the increase of pH, the adsorption efficiency decreased slightly. When pH is greater than pH_{pzc}, BC is negatively charged. The solution was now alkaline. MB ions are more likely to interact with OH⁻. A large amount of OH⁻ forms a whole around MB ions. This results in a weaker electrostatic repulsion between MB ions and BC. This is not conducive to the adsorption. When the pH is less than pH_{pzc}, the BC is positively charged. The solution was acidic at this time. MB ions are more easily combined with H⁺. MB ions with a lot of H⁺ around are more likely to combine with negative BC. And as the pH becomes smaller, this effect becomes more pronounced and the removal ratio is higher. However,

Table 2
Parameters of pseudo-first-order and pseudo-second-order kinetics models for MB onto three BCs

Samples	Pseudo-first-order model			Pseudo-second-order model			Experience
	k_1 (1/h)	Calculated q_e (mg/g)	R^2	k_2 (g/mg h)	Calculated q_e (mg/g)	R^2	q_e (mg/g)
BC700	0.74	2.33	0.8911	2.13	4.83	0.9995	4.78
BC500	0.65	1.20	0.8451	2.69	4.40	0.9996	4.40
BC300	0.600	1.03	0.7623	3.65	3.54	0.9990	3.62
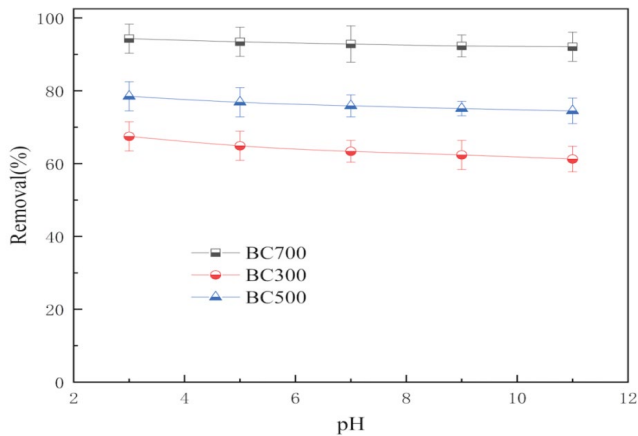
Fig. 6. Effect of pH by three BCs: MB removal (C_0 = 10 mg/L, adsorbent dose = 2.0 g/L, at 24 h and 25°C).

Fig. 7. Effect of adsorbent dose for the adsorption MB on three BCs (C_0 = 10 mg/L for MB, shaking time 24 h, at pH = 7.0 and 25°C).

due to the small amount of charge carried on the BC surface, the tendency for the removal ratio to decrease or increase is not obvious. Some studies have also shown that in the experiments of removing MB in water from fishbone BC and straw BC, the removal ratio did not change significantly with increasing pH [34,35]. The smaller amount of charge on the BC surface may explain the above results. This is similar to the conclusions obtained in this study In summary, the change in pH has a certain effect on the adsorption process. However, due to its weak effect, the electrostatic mechanism does not explain the main mechanism of BC adsorption of MB. At the same time, other experiments in this study were also performed in an environment of pH = 7.0.

3.4. Effect of adsorbent dose

The effect of the dose of BCs on the MB adsorption is indicated in Fig. 7. As the dose of adsorbent increases, the removal ratio of MB increases. When the adsorbent doses were increased from 0.8 to 3.0 g/L, the percentage of MB ions adsorbed by BC300 increased from 31.22% to 71.13%, and the percentage of MB ions adsorbed by BC500 increased from 52.80% to 84.15%. The percentage of MB ions adsorbed by BC500 increased from 86.68% to 95.60%. When the doses of adsorbent were more than 2.0 g/L, the MB removal ratio by the adsorbent was not significantly improved. Therefore, the optimal doses of BCs to adsorb MB were 2.0 g/L. The increase in adsorption efficiency is due to the increased effectiveness of the BCs binding site.

3.5. Effect of the ionic strength

At the same time, the influence of ion strength on the adsorption process was evaluated by adding NaCl, KCl, and MgCl$_2$. Fig. 8 shows that as the concentration of NaCl, KCl, and MgCl$_2$ in the solution decreases, the removal efficiency of MB on BC was first reduced. And then slightly increased at 0.1 mol/L of three salt solutions. The removal efficiencies of MB at NaCl concentrations of 0, 0.05, and 0.1 mol/L varied from 70.23% (BC300), 83.34% (BC500), and
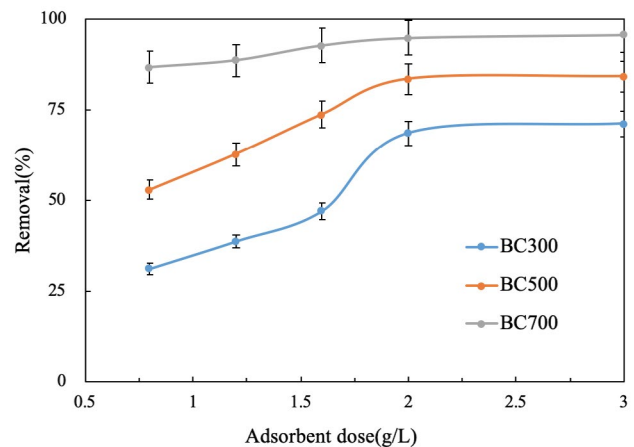
94.25% (BC700) to 66.27% (BC300), 73.38% (BC500), and 92.94% (BC700) onto the BC, respectively. And those of KCl varied from 69.26% (BC300), 82.54% (BC500), and 93.01% (BC700) to 65.03% (BC300), 80.02% (BC500), and 81.74% (BC700), respectively. Those of MgCl$_2$ varied from 69.26% (BC300), 82.54% (BC500), and 94.25% (BC700) to 50.43% (BC300), 72.02% (BC500), and 92.56% (BC700), respectively. As the ionic strength increases, the number of MB adsorbed on the BCs gradually decreased. The pH$_{pzc}$ values of BC500 and BC700 were 7.53 and 7.70, respectively. At a pH of 7.0, the surface of the BCs was predominantly positively charged. The sodium, potassium, or magnesium ions on BC500 and BC700 can interact with BCs to produce C$_\pi$–cations. Studies had shown that an unconventional bond might be established between the hydrogen (H$_3$O$^+$) and the electron cloud of the aromatic ring of the graphite layered on the carbon material [36]. Many alkaline carbon materials have one or several C$_\pi$ Lewis centers [37]. The C$_\pi$–cation interactions present were the main interaction forces. Additives (NaCl, KCl, and MgCl$_2$) appeared to be more prone to occupy adsorption sites on BCs. This led to a decrease in the adsorption capacity of BCs for MB. In some studies, some authors believed that the interaction with C$_\pi$–cations enhanced the adsorption capacity of Hg(II), Cd(II), and Cr(III) on positively charged ozone carbon material (alkaline carbon) [38–40]. At the same time, the presence of these ions also prevented the transfer of MB ions into the pores. Similar work has been described previously [41].

3.6. Adsorption isotherm

The adsorption isotherm type was predicted using the isotherm models of Langmuir and Friedrich, respectively. The parameters in Eqs. (5) and (6) were obtained from the adsorption isotherms of BC and are summarized in Table 3.

In Eq. (5), q_e (mg/g) is the equilibrium adsorption dose; Q_0 (mg/g) is the saturated adsorption dose; K_L (L/mg) is the adsorption equilibrium constant of the Langmuir isotherm; and C_e (mg/L) is the adsorption equilibrium concentration.
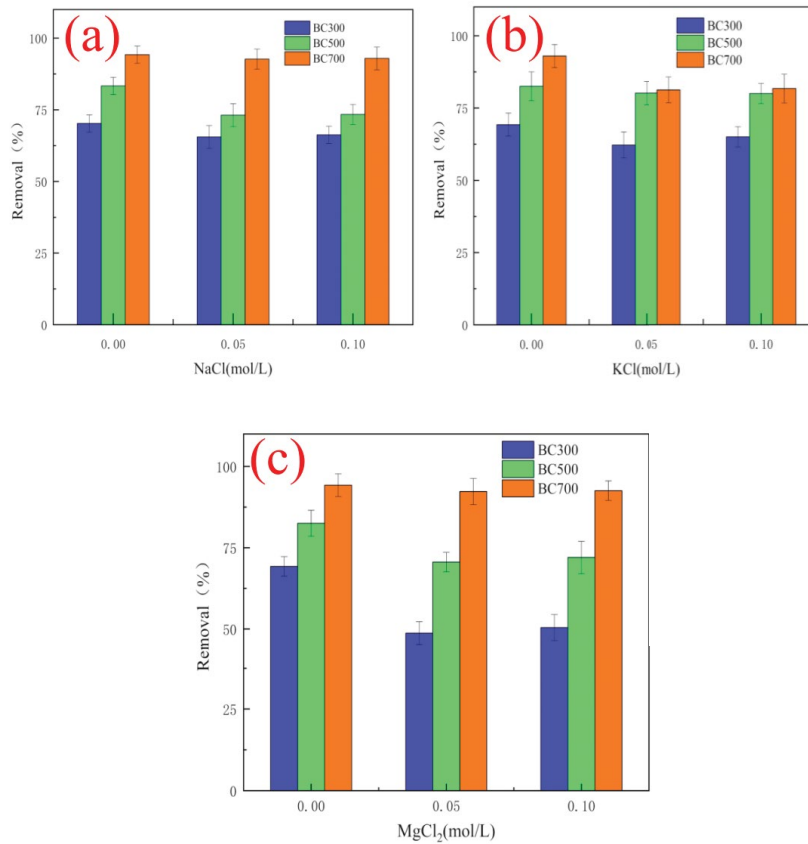
Fig. 8. Effect of ionic strength on the adsorption of MB on three BCs (C_0 = 10 mg/L, shaking time 24 h, adsorbent dose = 2.0 g/L, at pH = 7.0 and 25°C).

Table 3
Parameters of MB adsorption isotherms fitted with Langmuir and Freundlich models

Samples	Langmuir model			Freundlich model		
	Q_0 (mg/g)	K_L (L/mg)	R^2	K_F (L/mg)	$1/n$	R^2
BC700	7.75	2.94	0.9996	5.03	0.28	0.9144
BC500	6.37	2.36	0.9892	3.96	0.26	0.9623
BC300	5.18	2.17	0.9891	3.32	0.20	0.9320

$$q_e = \frac{Q_0 K_L C_e}{1 + K_L C_e} \tag{5}$$

In Eq. (6), K_F (L/mg) is a constant of the Freundlich isotherm, and the constant n is a parameter related to the adsorption strength, which varies depending on the nature of the material.

$$q_e = K_F C_e^{\frac{1}{n}} \tag{6}$$

As shown in Fig. 9a, the BC isothermal curve of MB was used to present a typical Langmuir type. As indicated in Fig. 9b, the calculations showed that the correlation coefficient according to the Langmuir model is greater than 0.99,

and the R^2 is greater than the R^2 of the Friedrich model. Therefore, the adsorption process conforms to the Langmuir isotherm model. The results show that the adsorption mechanism is related to the MB adsorption process in the case where the adsorption energy and the adsorption site are uniformly distributed on the surface of the adsorbent. Because the ordered carbon layer surface had uniform adsorption location and adsorption energy. At the same time, XRD results show that there are ordered carbon layers in the three BCs and the ordered carbon layers increase with the increase of temperature. Therefore, three results indicated that the adsorption of BC might be related to the presence of an ordered carbon layer. The surface of ordered carbon layer had uniform adsorption location and energy. At the same time, XRD results showed that there were ordered carbon layers in all three kinds of carbon. Therefore,
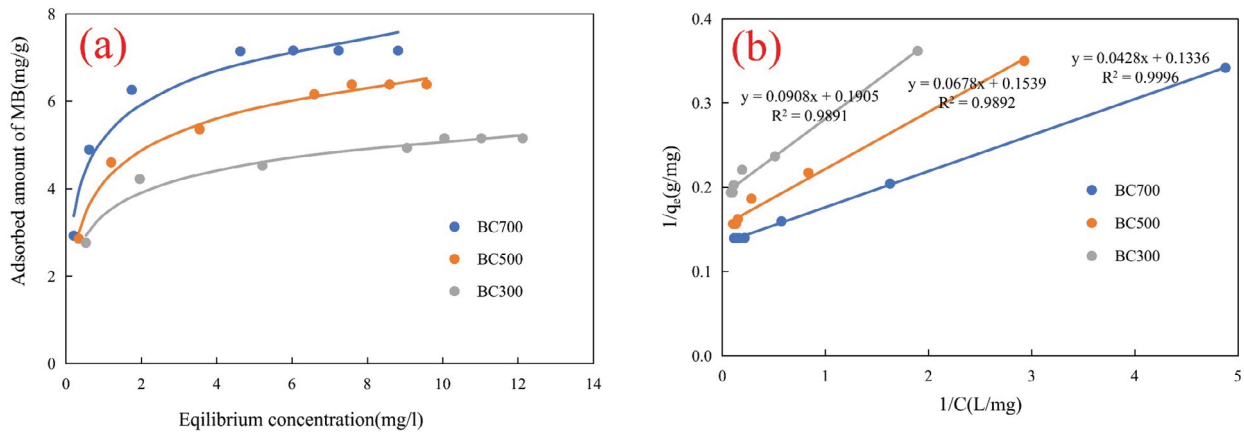
Fig. 9. Adsorption isothermal curve of MB on three BCs (C_0 = 6.056–20.254 mg/L, shaking time 24 h, adsorbent dose = 2.0 g/L, at pH = 7.0 and 25°C).

these two results indicated that the adsorption of MB on BC might be related to the existence of ordered carbon layer.

Table 3 lists the Q_0 and K_L parameters of MB obtained from the Langmuir isotherm which were 7.75 mg/g and 2.94 L/mg on BC700, 6.37 mg/g and 2.36 L/mg on BC500, and 5.18 mg/g and 2.17 L/mg on BC300, respectively. At the same time, the authors hypothesized that the interaction between BC (adsorbent) and MB ion (adsorbed molecule) was stronger because the surface of BC700 was more hydrophobic than BC500 and BC300, as described in the section of adsorption mechanism.

As shown in Table 4, the saturated adsorption amount of MB on BC was compared with various adsorbents [42–46]. The saturated adsorption capacity of this study was better than that of other adsorbents, such as pinewood BC (3.99 mg/g) [42], paper derived BC (1.66 mg/g) [42], rice hull BC (4.76 mg/g) [43], eucalyptus BC (2.06 mg/g) [44], palm bark BC (2.66 mg/g) [45], and 500°C common reed BC (5.03 mg/g) [46]. The saturated adsorption capacity of this study was lower than pH-sensitive hydrogel (49.10 mg/g). These comparisons in Table 4 illustrate that BCs have a higher saturated adsorption capacity for MB.

3.7. Thermodynamic analyses

The adsorption process was analyzed using thermodynamic indicators. In general, $\Delta G°$ is the amount of change in standard free energy (kJ/mol), $\Delta H°$ is the amount of change in standard enthalpy change (kJ/mol), and $\Delta S°$ is the amount of change in standard entropy change (J/mol k). The adsorption mechanism could use these data to estimate. The equation for calculating the thermodynamic parameters is as follows:

$$\Delta G° = -RT \ln \frac{C_{ad·e}}{C_e} \qquad (7)$$

$$\ln \frac{C_{ad·e}}{C_e} = \frac{\Delta S°}{R} - \frac{\Delta H°}{R} \frac{1}{T} \qquad (8)$$

Table 4
Maximum uptake capacity for the adsorption of MB onto various adsorbents

Adsorbents	Q_0 of MB (mg/g)	References
Pine wood BC	3.99	[42]
Paper derived BC	1.66	
Rice hull BC	4.76	[43]
Eucalyptus BC	2.06	[44]
Palm bark BC	2.66	[45]
500°C common reed BC	5.03	[46]
BC700	7.75	
BC500	6.37	This study
BC300	5.18	

where R is the gas constant (8.31 J/mol K); T is the temperature in Kelvin. $C_{ad·e}$ and C_e are the equilibrium concentrations of MB in the adsorbent and solution, respectively.

The values of $\Delta S°$ and $\Delta H°$ were determined by the intercept and slope of the van' Hoff plot, respectively ($\ln C_{ad·e}$ vs. $1/T$). Table 5 lists the values for $\Delta G°$, Table 5 showed the values of $\Delta G°$, which were calculated over BC were calculated to range from –9.21 kJ/mol (BC700), –4.69 kJ/mol (BC500), and –2.80 kJ/mol (BC300) to –5.25 kJ/mol (BC700), –2.65 kJ/mol (BC500), and –1.45 kJ/mol (BC300) for MB. It was worth noting that the $\Delta G°$ values were all negative, which showed that these processes were not only spontaneous but also feasible. The negative values for $\Delta H°$ (–5.35 kJ/mol (BC700), –1.88 kJ/mol (BC500), and –2.77 kJ/mol (BC300)) suggested that the process was exothermic. The positive value for $\Delta S°$ (13.68 J/mol k for BC700, 3.44 J/mol k for BC500 and 7.38 J/mol k for BC300) displayed that the affinity of the adsorbent for MB removal increased with the increase of randomness at the solid–liquid interface [47].

3.8. Desorption and regeneration

Results in Fig. 10 show two adsorption/regeneration cycles on BC, the absorbed MB was mostly released after

Table 5
Thermodynamic parameters for adsorption MB on three BCs

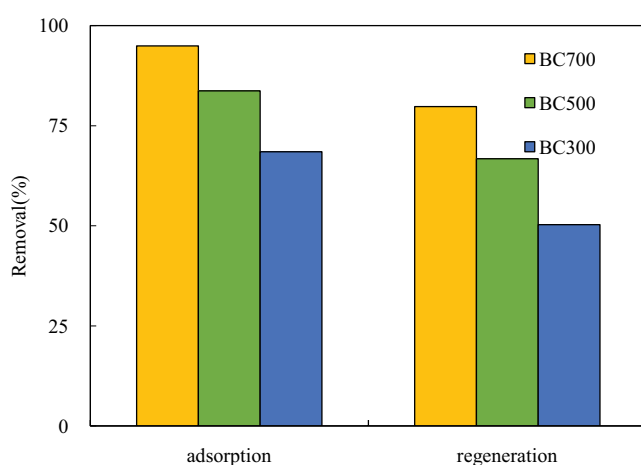| Samples	T (K)	$\Delta G°$ (kJ/mol)	$\Delta H°$ (kJ/mol)	$\Delta S°$ (J/mol k)
	308	−9.21		
BC700	298	−7.16	5.35	35.08
	273	−5.25		
	308	−4.69		
BC500	298	−4.12	2.77	18.47
	273	−2.65		
	308	−2.80		
BC300	298	−2.15	1.88	10.97
	273	−1.45		

Fig. 10. Adsorption desorption and regeneration removal of MB on two BCs (C_0 = 10 mg/L shaking time 24 h, adsorbent dose = 2.0 g/L, at pH = 7.0).

the regeneration, and the capacity for the MB absorption decreased by 15.12% and 17.00%, respectively. After two cycles of adsorption–elution, the adsorption capacity was regained largely and desorption ratio of the BC was maintained at around 84.00% and 80.00%, respectively. The results indicated that the MB loaded with the BC could be regenerated and be used repeatedly many times.

3.9. Adsorption mechanism

MB had a complex adsorption mechanism on BC. Hydrophobic, π–π interaction and hydrogen bonding can be the driving force of adsorption [48]. The results of the Langmuir and Freundlich models combined with BC_S (Table 3) and pH_{PZC} (Table 1a) of BCs indicated that electrostatic attraction was not the main adsorption mechanism of adsorption. For MB, the adsorption equilibrium constants on BC700 were higher than those of BC300 and BC500.

The hydrophobicity of BC can be used to explain the result. As displayed in Table 1a, the number of acidic functional groups of BC700 is less than that of BC300 and BC500. The adsorption experiments were conducted using BC300, BC500, and BC700. It showed that the number of acidic functional groups on BC500 and BC300 was found to

be 1.18 and 1.52 times that of BC700 (Table 1a). Therefore, BC700 with lower polarity on the surface has stronger hydrophobicity. According to FTIR analysis, it can be seen that the benzene peak on the BC surface has decreased and moved after adsorption. The hydrophobicity given to BC700 by the benzene peak may be involved in the adsorption process. At the same time, compared with BC300 and BC500, the peaks of various surface functional groups of BC700 are smaller. This is similar to the conclusion obtained from the measurement of the surface functional group described above. XRD analysis also shows that there is a locally ordered carbon layer inside the BC700. The diffraction peak of BC700 also shows that BC700 has strong aromaticity. This facilitates the development of hydrophobicity. The result of the K_L of BC700 (2.94 L/mg) showed larger than that of BC500 (2.36 L/mg) and BC300 (2.17 L/mg) (Table 3). Therefore, the adsorption strength (K_L) of BC700 might be explained by hydrophobic force that was dependent on the number of functional groups on the surface of the adsorbent and the degree of aromaticity. The hydrophobicity of the adsorbent surface is an important factor in measuring the adsorption capacity because there is a competition between water molecules and adsorbate at the adsorption point [49]. In water, the lower adsorption capacity of the adsorbent material may be caused by lower hydrophobicity. The adsorption equilibrium constant of BC700 is better than BC300 and BC500 because the former is more hydrophobic than the latter. Effective adsorption of moderately water-soluble substances (such as MB) on BC700 is better. The adsorption mechanism of MB is shown in Fig. 11.

The measurement results of surface functional groups and the results of FTIR also indicate that the acidic oxygen-containing functional groups on the surface of BC500 are abundant. Some studies have shown that the increase of electron-donating functional groups on the BC surface is more conducive to adsorption [33]. In the FTIR image of BC500, the carboxylic group (–C–COOH) on the surface of BC500 showed a downward trend after adsorption. The π–π interaction between MB and BC500 may explain this phenomenon. At the same time, XRD analysis results also show that BC500 has higher aromaticity. Higher aromaticity and increased electron-donating functional groups enhanced π–π interaction. This may be the main driving force for BC500 to adsorb MB.

However, BC300 had a great deal of oxygen-containing functional groups on its surface, including carboxylic groups, lactone groups, and phenolic groups (Table 1) [50]. In the analysis of FTIR and TGA, abundant oxygen-containing functional groups on the surface of BC300 were also found. The rich oxygen-containing functional groups on the surface of BC300 make it more hydrophilic. At the same time, FTIR and XRD analysis also showed that BC300 has lower aromaticity. Therefore, hydrophobicity and π–π interaction do not explain the mechanism of MB adsorption on BC300 [51]. FTIR analysis showed that the phenolic groups (–OH) peak on the BC300 surface decreased after adsorption. This may be due to the formation of hydrogen bonds between MB and phenolic groups (–OH) on the surface of BC300 (see Fig. 11). Similar studies have also reported that hydrogen bonding between carboxylic groups on the BC surface and MB also promotes adsorption [52]. This seems
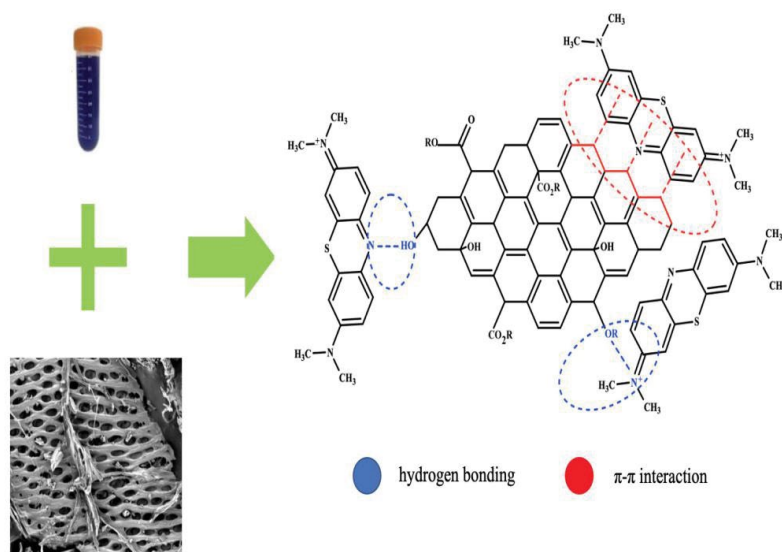
Fig. 11. Hydrophobic and hydrogen bond adsorption mechanism of carbon surface (a) hydrogen bonding and (b) π–π interaction.

to explain that hydrogen bonding is the main driving force for BC300 to adsorb MB.

4. Conclusions

The potential of three BCs as adsorbents to remove MB in aqueous solution was studied. The equilibrium data manifested that the adsorption thermodynamic process of MB was more in line with the Langmuir model. BC700 exhibits strong adsorption capacity in terms of adsorption of MB. The saturated adsorption capacities of BC700, BC500, and BC300 for MB were 7.75, 6.37, and 5.18 mg/g, respectively. Hydrogen bonding, π–π interaction, and hydrophobic force are the main adsorption mechanisms for BC adsorption of MB molecules. The results showed that chaff BC had greater potential as a wastewater treatment adsorbent for MB removal.

References

[1] A.B. Albadarin, J. Mo, Y. Glocheux, S. Allen, G. Walker, C. Mangwandi, Preliminary investigation of mixed adsorbents for the removal of copper and methylene blue from aqueous solutions, Chem. Eng. J., 255 (2014) 525–534.

[2] J.C.Y. Lo, M.A. Darracq, R.F. Clark, A review of methylene blue treatment for cardiovascular collapse, J. Emerg. Med., 46 (2014) 670–679.

[3] P. Nautiyal, K.A. Subramanian, M.G. Dastidar, Adsorptive removal of dye using biochar derived from residual algae after in-situ transesterification: alternate use of waste of biodiesel industry, J. Environ. Manage., 182 (2016) 187–197.

[4] W.A. Khanday, F. Marrakchi, M. Asif, B.H. Hameed, Mesoporous zeolite-activated carbon composite from oil palm ash as an effective adsorbent for methylene blue, J. Taiwan Inst. Chem. Eng., 70 (2017) 32–41.

[5] M.A. Islam, S. Sabar, A. Benhouria, W.A. Khanday, M. Asif, B.H. Hameed, Nanoporous activated carbon prepared from karanj (Pongamia pinnata) fruit hulls for methylene blue adsorption, J. Taiwan Inst. Chem. Eng., 74 (2017) 96–104.

[6] F. Marrakchi, M.J. Ahmed, W.A. Khanday, M. Asif, B.H. Hameed, Mesoporous-activated carbon prepared from chitosan flakes via single-step sodium hydroxide activation for the adsorption of methylene blue, Int. J. Biol. Macromol., 98 (2017) 233–239.

[7] M. Ejder-Korucu, A. Gürses, C. Doǧar, S.K. Sharma, M. Acıkyıldız, Removal of Organic Dyes from Industrial Effluents: An Overview of Physical and Biotechnological Applications, Vol. 12, S.K. Sharma, Ed., Green Chemistry for Dyes Removal from Wastewater: Research Trends and Applications, Scrivener Publishing & Wiley, Beverly, MA, 2015, pp. 1–3.

[8] S. Jia, D. Tang, J. Peng, X. Yang, Z. Sun, Crosslinked electrospinning fibers with tunable swelling behaviors: a novel and effective adsorbent for methylene blue, Chem. Eng. J., 124 (2020) 472–515.

[9] D. Mohan, A. Sarswat, Y.S. Ok, C.U. Pittman, Organic and inorganic contaminants removal from water with biochar, a renewable, low cost and sustainable adsorbent - a critical review, Bioresour. Technol., 160 (2014) 191–202.

[10] F. Rozada, L.F. Calvo, A.I. García, J. Martın-Villacorta, M. Otero, Dye adsorption by sewage sludge-based activated carbons in batch and fixed-bed systems, Bioresour. Technol., 87 (2003) 221–230.

[11] G. Agegnehua, A.K. Srivastavab, M.I. Bird, The role of biochar and biochar compost in improving soil quality and crop performance: a review, Appl. Soil Ecol., 119 (2017) 156–170.

[12] F. Lian, G. Cui, Z. Liu, L. Duo, G. Zhang, B. Xing, One-step synthesis of a novel N-doped microporous biochar derived from crop straws with high dye adsorption capacity, J. Environ. Manage., 176 (2016) 61–68.

[13] X. Yao, L. Ji, J. Guo, S. Ge, W. Lu, L. Cai, Y. Wang, W. Song, H. Zhang, Magnetic activated biochar nanocomposites derived from wakame and its application in methylene blue adsorption, Bioresour. Technol., 302 (2020) 122–138.

[14] W. Huang, Y. Chen, J.Q. Zhang, C. Lei, Y.P. Wang, Q.T. Ye, Adsorption characteristics of methylene blue on corn cob-based and sheep manure-based biochar, Chin. Water Treat. Technol., 44 (2018) 74–80.

[15] P.H. Zhang, Y.C. Li, H.B. Hu, J.G. Zhao, J.S. Wang, Adsorption of methylene blue by Ginkgo biloba biochar, Environ. Pollut. Prev., 39 (2017) 1229–1234.

[16] H. Zhang, Preparation and Adsorption Properties of Hydrothermal Activated Carbon from Walnut Shell, Ph.D. Dissertation, Dalian University of Technology, 2016.

[17] X. Han, L. Chu, S. Liu, T. Chen, C. Ding, J. Yan, L. Cui, G. Quan, Removal of methylene blue from aqueous solution using porous biochar obtained by KOH activation of peanut shell biochar, BioResources, 10 (2016) 2836–2849.

[18] Y. Xu, Y. Liu, S. Liu, X. Tan, G. Zeng, Y. Ding, W. Cao, B. Zheng, Enhanced adsorption of methylene blue by citric acid modification of biochar derived from water hyacinth (*Eichornia crassipes*), Environ. Sci. Pollut. Res. Int., 23 (2016) 23606–23618.

[19] H. Yu, B. Lv, H. Chen, Utilization status and prospect of solid organic waste based on edible fungi, Chin. Agric. Sci. Bull., 30 (2014) 305–309.

[20] W. Liu, X. Zhu, L. Zhang, Adsorption of methylene blue in water by modified fungal bran, J. Tianjin Univ. Technol., 36 (2017) 39–44.

[21] Y.W. Ma, X. Yang, P. Li, H.Y. Li, Q.L. Zhang, L.Q. Zhang, Study on adsorption characteristics of crystal violet on modified mushroom bran, J. New Chem. Mat. Chin., 44 (2016) 241–244.

[22] X. Zhang, Study on Preparation and Characterization of Hydrothermal Bacterial Charcoal, MA, Dissertation, Zhejiang Institute of Technology, 2019.

[23] X. Zhang, J. Lou, J. Su, Y. Zhang, S. Liu, Biochar preparation and physicochemical properties of Xiuzhen mushroom bran, J. Zhejiang Univ. Sci. Technol., 31 (2019) 50–57.

[24] C.A. Leon, J.M. Solar, V. Calemma, L.R. Radovic, Evidence for the protonation of basal plane sites on carbon, Carbon, 30 (2016) 797–811.

[25] Z. Wu, P.A. Webley, D. Zhao, Comprehensive Study of pore evolution, mesostructural stability, and simultaneous surface functionalization of ordered mesoporous carbon (FDU–15) by wet oxidation as a promising adsorbent, Langmuir, 26 (2016) 10277–10286.

[26] M.V. López-Ramón, F. Stoeckli, C. Moreno-Castilla, F. Carrasco-Marín, On the characterization of acidic and basic surface sites on carbons by various techniques, Carbon, 37 (2017) 1215–1221.

[27] P. Zhang, Y. Li, Y. Cao, L. Han, Characteristics of tetracycline adsorption by cow manure biochar prepared at different pyrolysis temperatures, Bioresour. Technol., 285 (2019) 121–348.

[28] L.M. Mosley, P. Willson, B. Hamilton, G. Butler, R. Seaman, The capacity of biochar made from common reeds to neutralise pH and remove dissolved metals in acid drainage, Environ. Sci. Pollut. Res., 22 (2015) 15113–15122.

[29] J.H. Yuan, R.K. Xu, H. Zhang, The forms of alkalis in the biochar produced from crop residues at different temperatures, Bioresour. Technol., 102 (2011) 3488–3497.

[30] K. Komnitsas, D. Zaharaki, G. Bartzas, G. Kaliakatsou, A. Kritikaki, Efficiency of pecan shells and sawdust biochar on Pb and Cu adsorption, Desal. Water Treat., 57 (2016) 3237–3246.

[31] Y. Liu, X. Zhao, J. Li, D. Ma, R. Han, Characterization of biochar from pyrolysis of wheat straw and its evaluation on methylene blue adsorption, Desal. Water Treat., 46 (2012) 115–123.

[32] B. Singh, B.P. Singh, A.L. Cowie, Characterisation and evaluation of biochar for their application as a soil amendment, Soil Res., 48 (2010) 516–525.

[33] M.J. Ahmed, P.U. Okoye, E.H. Hummadi, B.H. Hameed, High-performance porous biochar from the pyrolysis of natural and renewable seaweed (*Gelidiella acerosa*) and its application for the adsorption of methylene blue, Bioresour. Technol., 278 (2019) 159–164.

[34] W. Wang, Study on the Preparation of Fishbone Charcoal and Application as the Adsorbent for Pb(II) and Methylene Blue, Ph.D. Dissertation, Wuhan University of Technology, 2017.

[35] X. Ji, L. Lv, Sorption properties and mechanisms of organic dyes by straw biochar, Acta Sci. Circumstatiae, 36 (2016) 1648–1654.

[36] M.A. Montes-Moran, J. Angel Menendez, E. Fuente, D. Suarez, Contribution of the basal planes to carbon basicity: an abinitio study of the H_3O^+–π interactions in cluster model, J. Phys. Chem. B, 102 (1998) 5595–5601.

[37] L.R. Radovic, C. Moreno-Castilla, J. Rivera-Utrilla, Chapter 4: Carbon Materials as Adsorbents in Aqueous Solutions, Vol. 27, L.R. Radovic, Ed., Chemistry and Physics of Carbon, Marcel Dekker, New York, NY, 2001, pp. 227–405.

[38] D.A. Dougherty, Cation–π interactions in chemistry and biology: a new view of benzene Phe, Tyr, and Trp, Science, 271 (2016) 163–168.

[39] J. Rivera-Utrilla, M. Sánchez-Polo, Adsorption of Cr(III) on ozonised activated carbon, Importance of Cπ–cation interactions, Water Res., 37 (2003) 335–3340.

[40] M. Sanchez-Polo, J. Rivera-Utrilla, Adsorbent-adsorbate interactions in the adsorption of Cd(II) and Hg(II) on ozonised activated carbons, Environ. Sci. Technol., 36 (2002) 3850–3854.

[41] M.A. Alvarez-Merino, V. Lopez-Ramon, C. Moreno-Castilla, A study of the static and dynamic adsorption of Zn(II) ions on carbon materials from aqueous solutions, J. Colloid Interface Sci., 288 (2005) 335–341.

[42] L. Lonappan, T. Rouissi, R.K. Das, S.K. Brar, A.A. Ramirez, M. Verma, R.Y. Surampalli, J.R. Valero, Adsorption of methylene blue on biochar microparticles derived from different waste materials, Waste Manage., 49 (2016) 537–544.

[43] G.B. Lee, H.J. Kim, S.G. Park, Y.S. Ok, J.H. Ahn, Comparison of adsorption properties of activated carbon and biological tea in removal of methyl blue, J. Korean Soc. Water Environ., 3203 (2016) 291–296.

[44] M.Y. Zhang, F.M. Li, The adsorption research of biochar prepared from common red on methylene blue, J. Ocean Univ., 46 (2016) 96–103.

[45] L. Sun, S.G. Wan, W.S. Luo, Biochar prepared from anaerobic digestion residue, palm bark, and eucalyptus for adsorption of cationic methylene blue dye: characterization, equilibrium, and kinetic studies, Bioresour. Technol., 140 (2013) 406–413.

[46] H. Zheng, Z. Wang, X. Deng, J. Zhao, Y. Luo, J. Novak, S. Herbert, B. Xing, Characteristics and nutrient values of produced from giant reed at different temperatures, Bioresour. Technol., 130 (2017) 463–471.

[47] P. Luo, Y. Zhao, B. Zhang, J. Liu, Y. Yang, J. Liu, Study on the adsorption of neutral red from aqueous solution onto halloysite nanotubes, Water Res., 44 (2010) 1489–1497.

[48] C. Moreno-Castilla, Adsorption of organic molecules from aqueous solutions on carbon materials, Carbon, 42 (2004) 83–94.

[49] R. Voss, Mesoporous Organosilica Materials with Amine Functions: Surface Characteristics and Chirality, Ph.D. Dissertation, Potsdam University, 2005.

[50] G. Li, W. Zhu, C. Zhang, S. Liu, L. Zhu, W. Zhao, Effect of a magnetic field on the adsorptive removal of methylene blue onto wheat straw biochar, Bioresour. Technol., 206 (2016) 16–22.

[51] Y. Chun, G. Sheng, C. Chiou, B. Xing, Compositions and sorptive properties of crop residue-derived chars, Environ. Sci. Technol., 38 (2004) 4649–4655.

[52] L. Sun, D. Chen, S. Wan, Z. Yu, Performance, kinetics, and equilibrium of methylene blue adsorption on biochar derived from eucalyptus saw dust modified with citric, tartaric, and acetic acids, Bioresour. Technol., 198 (2015) 300–308.